A Gas-Phase Study of the Kinetics of Formation of $Fe(CO)_3DMB$, $Fe(CO)_3(DMB)_2$, and $Fe(CO)_4DMB$: The Bond Dissociation Enthalpy for $Fe(CO)_3(DMB)_2$ (DMB = 3,3-dimethyl-1-butene)

Jiaqiang Wang and Eric Weitz*

Department of Chemistry, Northwestern University, Evanston, Illinois 60208-3113

Received: January 7, 2001; In Final Form: March 6, 2001

The transient spectra of $Fe(CO)_3$(3,3-dimethyl-1-butene) and $Fe(CO)_3$(3,3-dimethyl-1-butene)$_2$ have been obtained in the carbonyl stretching region of the infrared. $Fe(CO)_4$(3,3-dimethyl-1-butene) has also been monitored. The bond dissociation enthalpy for loss of 3,3-dimethyl-1-butene (DMB) from $Fe(CO)_3(DMB)_2$ has been determined as 15.2 ± 3.8 kcal mol^{-1}. The rate constants for the reactions of $Fe(CO)_3$ + DMB, $Fe(CO)_3DMB$ + DMB, $Fe(CO)_4$ + DMB, and $Fe(CO)_3DMB$ + CO have been measured as $(9.6 \pm 1.4) \times 10^{-11}$, $(2.3 \pm 0.8) \times 10^{-12}$, $(5.0 \pm 0.5) \times 10^{-13}$, and $(3.9 \pm 0.6) \times 10^{-12}$ cm^3 molecule^{-1} s^{-1}, respectively. The effects of the polarizability and steric interaction energy of the ligand on the bimolecular rate constants for the reactions of $Fe(CO)_3L$ + L (L = olefin) complexes are discussed. A correlation between these rate constants and the steric interaction energy divided by the magnitude of the polarizability of the ligand is observed. An estimate for the rate constant for addition of 1-pentene to $Fe(CO)_3$(1-pentene), based on data and correlations from this study, does not lead to a significant change in calculated thermodynamic parameters for processes relevant to the isomerization of pentene. Factors that could influence the stability of $Fe(CO)_3L_2$ complexes are also discussed.

I. Introduction

Coordinatively unsaturated metal carbonyls are involved in a variety of stoichiometric and catalytic processes including: olefin isomerization, hydrogenation, hydrosilation, and hydroformylation.[1−4] A detailed understanding of the kinetics and mechanisms for such processes requires the elucidation of rate constants for individual microscopic steps that take place in a complex kinetic mechanism, as well as the determination of thermochemical information for reaction products and reaction intermediates. Though considerable progress has been made in understanding the kinetics and reaction mechanisms of coordinatively unsaturated metal carbonyls, and some information is available on bond dissociation energies, there is still rather limited information in these areas.

Time-resolved infrared spectroscopy is a technique that has been successfully used to delineate the microscopic kinetic processes that are part of complex kinetic mechanisms.[5−8] For example, real time kinetic information on the iron carbonyl-catalyzed isomerization of propene and 1-pentene, in the gas phase, has been obtained.[7,8] It has been generally accepted that iron carbonyl-induced olefin isomerization involves a β-hydrogen transfer process, and this has been demonstrated for propene and 1-pentene, both of which contain allylic hydrogens. When a β-hydrogen is present on the olefin, a rapid β-hydrogen transfer process can occur, leading to formation of a π-allyl hydride. When such a species forms rapidly after the rate limiting addition of an olefin to a moiety that otherwise could coordinate with a pair of olefin ligands, a direct measurement of the rate constant for association of the second olefin is effectively precluded. As such, in the systems discussed above, the rate constant for addition of an olefin to the $Fe(CO)_3$(olefin) adduct was, by necessity, estimated. This estimate was based on the rate constant for addition of ethylene and propene to $Fe(CO)_3$(ethylene). Since ethylene does not contain β-hydrogens, such a measurement could be made for this adduct.

However, there is little detailed information about the variation of rate constants for the reaction of $Fe(CO)_3L$ + L as a function of the size of an olefin (L). Thus, it is not clear if this estimate is valid for larger olefins such as pentene. Since both the kinetics and thermodynamics of the olefin isomerization process are directly tied to the magnitude of this rate constant, additional studies of the kinetics of addition of olefins to $Fe(CO)_3$(olefin) complexes seem warranted. An obvious system, in which β-hydrogen transfer is precluded, is 3,3-dimethyl-1-butene. This system, which lacks β-hydrogens, provides an opportunity to obtain data on the effect of increasing molecular size on the kinetics of olefin addition to coordinatively unsaturated iron carbonyls.

In addition, though conventional wisdom indicates that the bond energy for olefins bound to metal carbonyls should decrease as the "size" of the olefin increases,[1] there is little actual data in this area—particularly in the gas phase where solvent effects are not operative.

In this study we have measured microscopic rate constants for the addition of DMB to coordinatively unsaturated iron carbonyls. These measurements provide additional information about the dependence of such rate constants on the size of the olefin, and on the factors that control their magnitude. An interesting correlation is observed between the magnitude of the addition rate constant and the steric interaction energy divided by the polarizability of the incoming ligand. The bond dissociation enthalpy (BDE) for $Fe(CO)_3(DMB)_2$ has been measured and data has been obtained on the stability of $Fe(CO)_4$(DMB). In addition, the effect of a change in the

* Author to whom correspondence should be addressed.

10.1021/jp010061z CCC: $20.00 © 2001 American Chemical Society
Published on Web 05/08/2001

magnitude of the rate constant for addition of a second olefin to $Fe(CO)_3$olefin on the thermodynamics of the olefin isomerization process is calculated.

II. Experimental Section

The time-resolved IR apparatus used in this study has been described in detail in refs 6 and 9. This study used two different infrared probes. Reactions occurring on either a microsecond or millisecond time scale were monitored by a tunable diode laser. The beam from this laser was double passed through a 42 cm long, 2.5 cm diameter static gas sample cell terminated with CaF_2 windows, and was then focused onto the element of a fast InSb detector, which has a minimum intrinsic response time of ~250 ns. The signal from the InSb detector was amplified and sent to a digital oscilloscope, where it was digitized and averaged for 10−15 traces. The photolysis source in these experiments was the 308 nm output of an excimer laser, operating on XeCl.

With the diode laser as the probe source, time-resolved infrared spectra were constructed from waveforms acquired at probe frequencies within the carbonyl stretch region by joining together the amplitude of various waveforms at common delay times. Kinetic information was determined from transients at a particular probe frequency, as a function of the pressure of the reactant of interest. These signals were fit to exponentials using commercial software.

Reactions occurring on time scales of minutes or longer were followed with a time-resolved FTIR spectrometer operating in the "GC" mode. In this mode a spectrum of the cell contents could be acquired at predetermined time intervals after photolysis. Using this method, spectra were obtained in the 1900−2200 cm^{-1} region at 8 cm^{-1} resolution with ~10 to 15 spectrometer scans. The cell contents were allowed to thermally equilibrate and mix for 30 minutes before being photolyzed for ~20 s with the 355 nm, 10 Hz output of a frequency-tripled Nd:YAG laser. Both the YAG laser and the excimer laser delivered ~6 mJ/cm^2 at the front window of the sample cell. Unless specifically indicated, all experiments were performed at a cell temperature of (24 ± 1) °C. Except where otherwise noted, all errors are reported as 2σ from linear regression fits.

The BDE of $Fe(CO)_3(DMB)_2$ was measured using static cell fills of 0.050 Torr $Fe(CO)_5$, ~10 to150 Torr DMB, and ~5.3 to 31 Torr CO, and enough He to bring the total pressure to at least 80 Torr. Rate constants for the ligand association reactions were measured under the following conditions in a static cell: $Fe(CO)_3$ + DMB, 0.040−0.050 Torr $Fe(CO)_5$ and 20−300 mTorr DMB; $Fe(CO)_3DMB$ + DMB, 0.05 Torr $Fe(CO)_5$ and 50 to 500 mTorr DMB (decay at 2071 cm^{-1}), or 0.5 to ~2.0 Torr DMB (growth at 1986 cm^{-1}); $Fe(CO)_3DMB$ + CO, at 2006 cm^{-1}, 50 mT $Fe(CO)_5$, 0.5Torr DMB and 1 to ~4.0 Torr CO; at 2071 cm^{-1}, 0.5 Torr DMB, and 0.1 to ~1 Torr CO; $Fe(CO)_4$ + DMB, at 2090 cm^{-1}, 50 mT $Fe(CO)_5$, 0.05−0.75 Torr DMB, and ~5.5 Torr CO; at 2001 cm^{-1}, 0.05−0.75 Torr DMB and ~5.5 Torr CO. For all of these experiments, enough He was added to bring the total pressure up to at least 80 Torr. Experiments were performed to ensure that the conditions under which rate constants were measured corresponded to the high-pressure limit for the bimolecular reactions under study.[5,6]

$Fe(CO)_5$ of 99+% purity was obtained from Aldrich Chemical. DMB specified as 98.4% was obtained from Chemsampco. These compounds were put through a series of freeze−pump−thaw cycles before use. The following gases were obtained from Matheson at the stated purities and used as received: CO, 99.9%; He, 99.999%.

III. Results

A. $Fe(CO)_3(DMB)$, $Fe(CO)_3(DMB)_2$, and $Fe(CO)_4DMB$ Absorptions. The 308-nm photolysis of $Fe(CO)_5$ produces $Fe(CO)_3$ as the only detectable product.[8,10−12] The expected association reactions for $Fe(CO)_3$ produced in the presence of $Fe(CO)_5$ and DMB are as follows:

$$Fe(CO)_3 + DMB \xrightarrow{k_1} Fe(CO)_3DMB \quad (1)$$

$$Fe(CO)_3DMB + DMB \xrightarrow{k_2} Fe(CO)_3(DMB)_2 \quad (2)$$

$$Fe(CO)_3 + Fe(CO)_5 \xrightarrow{k_3} Fe_2(CO)_8 \quad (3)$$

$$Fe(CO)_3DMB + Fe(CO)_5 \xrightarrow{k_4} Fe_2(CO)_8DMB \quad (4)$$

Since DMB has no allylic hydrogens, formation of a π-allyl hydride complex is not expected after addition of DMB to $Fe(CO)_3$. The first anticipated olefin adduct in this system is the η^2-bound olefin complex $Fe(CO)_3DMB$, shown in eq 1. After its formation, $Fe(CO)_3DMB$ can add DMB to form $Fe(CO)_3(DMB)_2$, as in eq 2. As will be discussed below, a spectrum of the system taken shortly after photolysis can have contributions from both $Fe(CO)_3DMB$ and $Fe(CO)_3(DMB)_2$. Thus, it is easier to begin the discussion of assignments of absorptions with a longer time spectrum, where experimental conditions have been arranged such that the spectrum is expected to be dominated by absorptions of $Fe(CO)_3(DMB)_2$.

$Fe(CO)_3(DMB)_2$ is expected to form via reaction 2 and its absorptions can be optimized by increasing the DMB pressure, which minimizes the amount of polynuclear species formed by reactions 3 and 4, and by obtaining a spectrum on a time scale that is long enough that virtually all the initially formed $Fe(CO)_3(DMB)$ has reacted with DMB. Figure 1A shows such a spectrum obtained for a DMB pressure of 2.0 Torr.

To our knowledge DMB adducts of $Fe(CO)_3$ and $Fe(CO)_4$ have not been previously reported. Therefore, we refer to the spectra of the analogous DMP (dimethyl-1-pentene) adducts, which are expected to be similar to the spectra of the DMB (3,3,-dimethyl-1-butene) complexes under investigation. Thus, the known spectrum of the products of reaction of $Fe(CO)_3$ with DMP can be used to predict the positions of the expected absorption of the product(s) of reaction of $Fe(CO)_3$ with DMB. $Fe(CO)_3(DMP)_2$ has absorptions at 2046 (1.0) and 1970 cm^{-1} (15)[13] (numbers in parentheses are relative absorbances) in a 3-methylpentene glass at 90 K. Taking into account the expected shift to higher frequency for absorption bands in the gas phase relative to a hydrocarbon glass, which is typically in the range of 10−20 cm^{-1}, the gas-phase absorptions of $Fe(CO)_3(DMB)_2$ would be expected at ~2061 and 1985 cm^{-1}, respectively. Absorptions are observed in the spectrum in Figure 1A at 1986 and 2060 cm^{-1} which are assigned to $Fe(CO)_3(DMB)_2$. Unlike the reports of the solution spectrum of $Fe(CO)_3(DMP)_2$, $Fe(CO)_3(DMB)_2$ also has a weak absorption at ~1974 cm^{-1}. Interestingly, $Fe(CO)_3(C_2H_4)_2$ also has 3 absorption bands: 2069, 2001, and 1997 cm^{-1}.[14] The kinetics of formation of $Fe(CO)_3(DMB)_2$ were probed at 1986 cm^{-1}, since this is the strongest of the absorptions.

We now turn our attention to $Fe(CO)_3DMB$. $Fe(CO)_3DMP$ has absorptions at 2041, 1966, and 1953 cm^{-1} in a 3-methylpentene glass.[13] The corresponding $Fe(CO)_3DMB$ absorptions in the CO stretching region, in the gas phase, would be anticipated at ~2055, 1980, and 1967 cm^{-1}. In addition, the

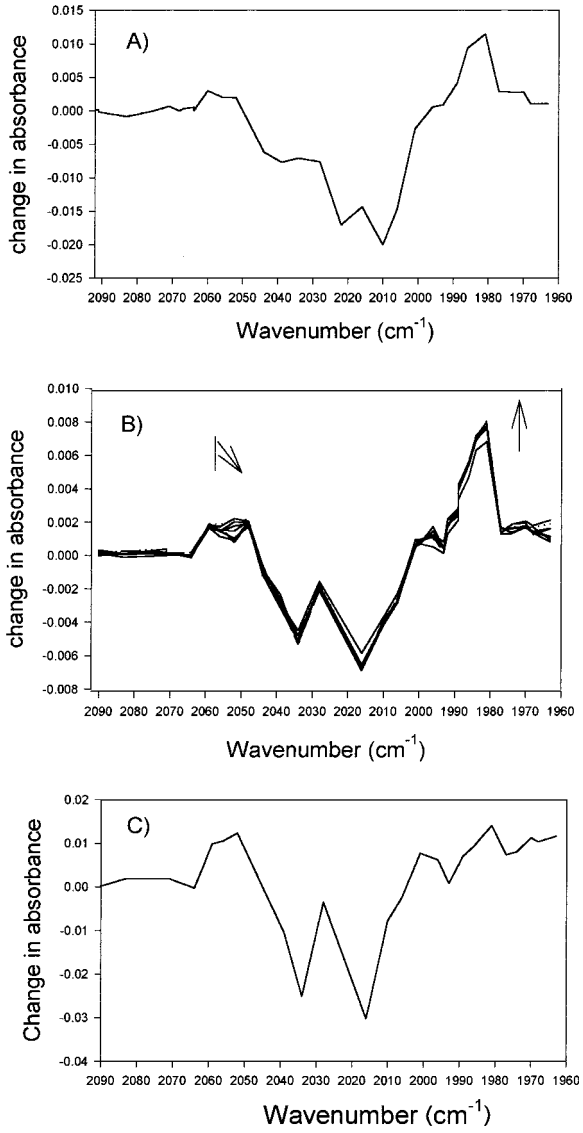

Figure 1. (A) Time-resolved infrared spectra at 45 μs after 308 nm photolysis of a mixture of 50 mTorr $Fe(CO)_5$, 2 Torr DMB, and 85 Torr He. (B) Time-resolved infrared spectra generated upon 308 nm photolysis of a mixture of 50 mTorr $Fe(CO)_5$, 0.3 Torr DMB, and 86 Torr He. The spectra cover a total time range of 80 μs with each successive trace incremented by 10 μs, with the first trace 10 μs after the laser pulse. The arrows indicate the direction of evolution of the traces at the relevant wavelengths. (C) The result of subtraction of (A) from the spectrum in (B), obtained at 20 μs after photolysis. See text for assignments.

absorptions of $Fe(CO)_3$DMB would also be anticipated to be close to those of $Fe(CO)_3C_2H_4$, which, based on data in refs 13 and 15, are expected at ~2052, 1989, and 1963 cm^{-1} in the gas phase.

The time-resolved infrared spectra produced by 308 nm photolysis of a mixture of 50 mTorr $Fe(CO)_5$ in the presence of 0.3 Torr DMB and 84 Torr He, over the time scale of 20−200 μs, is shown in Figure 1B. In this figure there are multiple absorptions present, including a broad feature in 2045−2062 cm^{-1} region. As indicated above, $Fe(CO)_3$DMB should have an absorption in this region. In addition, $Fe_2(CO)_8$ with an absorption at ~2048 cm^{-1} is known to form via reaction 3. Based on the known rate constant[10] for reaction 3 and the rate constant obtained in this study for reaction 1 (vide infra), it is clear that production of $Fe_2(CO)_8$ is significant under the conditions for which the spectrum in Figure 1B was obtained, and $Fe_2(CO)_8$ absorbs in the lower energy portion of the broad absorption in the 2045−2062 cm^{-1} region. Production of $Fe_2(CO)_8$ can be minimized by addition of more DMB. However, under these conditions there will be significant $Fe(CO)_3(DMB)_2$ present. This is apparent if one compares the intensity of the absorption at 1986 cm^{-1} to the intensity of the absorption in the 2045−2062 cm^{-1} region. In Figure 1B the absorption at 1986 cm^{-1} is much more intense than the absorption in the 2045−2062 cm^{-1} region, as it is in Figure 1A. However, based on matrix data and on the spectrum we obtain for $Fe(CO)_3$(DMB) (see Figure 1C and associated text later in this section), the intensities of the absorptions of $Fe(CO)_3$(DMB) at 2056 and 1981 cm^{-1} are approximately equal. Thus, the more intense band at 1984 cm^{-1} in Figure 1B results from the overlap of absorptions of $Fe(CO)_3$(DMB) and $Fe(CO)_3(DMB)_2$.

As a result of this overlap, the spectrum of $Fe(CO)_3$DMB can best be obtained by subtracting a spectrum which contains absorptions that are dominated by $Fe(CO)_3(DMB)_2$, as in Figure 1A, from the spectrum in Figure 1B. The result is shown in Figure 1C. The absorptions in Figure 1C, at 1970, ~1981, and ~2056 cm^{-1}, are close to the positions predicted for the absorptions of $Fe(CO)_3$(DMB) and are assigned to $Fe(CO)_3$DMB. For each of these absorptions there is an absorption of $Fe(CO)_3(DMB)_2$ at a similar energy (1974, 1986, and 2060 cm^{-1}). Therefore, all of the absorptions of $Fe(CO)_3$DMB are expected to be convoluted with those of $Fe(CO)_3(DMB)_2$.

Based on the shapes and intensities of individual transients (Figure 2), a diode probe wavelength of 2071 cm^{-1} (Figure 2.A) was an optimal compromise for minimizing overlap of the $Fe(CO)_3$(DMB) and $Fe_2(CO)_8$ absorptions and maximizing the relative absorbance of $Fe(CO)_3$(DMB). The rate constant for reaction of $Fe(CO)_3$ with DMB was probed by monitoring the DMB-dependent rise of $Fe(CO)_3$(DMB) at 2071 cm^{-1} (the inset in Figure 2.A). Ideally, this reaction could also have been followed by monitoring the DMB dependent fall of $Fe(CO)_3$. However, the output of the diode laser used in this experiment was weak and noisy in the 1953 cm^{-1} region, where $Fe(CO)_3$ absorbs, which effectively precluded probing this reaction by monitoring the loss of $Fe(CO)_3$.

When the absorptions of a species that is reacting to form another species overlap with the absorptions of a product of the reaction, the shape of the observed transient signal depends on the relative absorbances of the bands of the two overlapping species. At 1986 cm^{-1} only the growth of $Fe(CO)_3(DMB)_2$ is observed (Figure 2B), indicating that $Fe(CO)_3(DMB)_2$ is the stronger absorber at this wavelength.

Photolysis of $Fe(CO)_5$ at either 355 or 351 nm is expected to produce an ~60:40 mixture of $Fe(CO)_3$ and $Fe(CO)_4$.[12] When a mixture of 0.1 Torr $Fe(CO)_5$, 20 Torr DMB,and 80 Torr CO is photolyzed, $Fe(CO)_4$(DMB), which can be formed from $Fe(CO)_3$ via either of two pathways, or from $Fe(CO)_4$, will be the dominant stable olefin adduct. An FT-IR spectrum produced by Nd:YAG laser (355 nm) photolysis of a mixture of 0.1 Torr $Fe(CO)_5$, 20 Torr DMB and 80 Torr CO is shown in Figure 3. The absorptions of residual $Fe(CO)_5$ have been subtracted from a spectrum recorded immediately following photolysis of the above mixture. Once again, the known spectrum of the analogous $Fe(CO)_4$DMP complex can be used to predict the positions of the absorptions expected for $Fe(CO)_4$DMB. In 3-methylpentane solution, $Fe(CO)_4$(3,3-dimethyl-1-pentene) has absorptions at 2079 (1.0), 1997 (4.0), and 1978 (3.0),[13] with a shoulder on the 1997 cm^{-1} absorption at 2003 cm^{-1}. The positions of these absorptions lead to a prediction of gas-phase

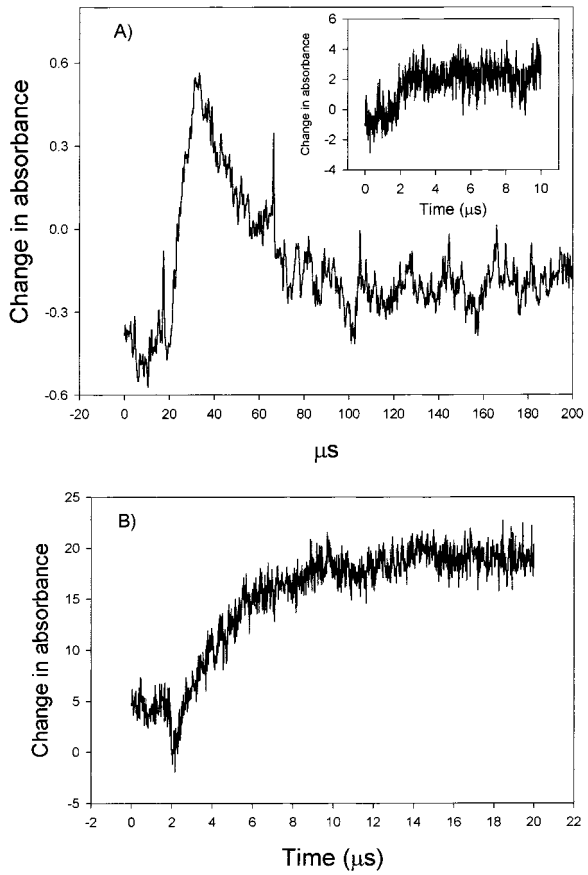

Figure 2. Typical transient absorption signals: (A) Decay of $Fe(CO)_3DMB$ monitored at 2071 cm^{-1} after photolyzing 50 mTorr $Fe(CO)_5$ in the presence of 0.3 Torr DMB and 82 Torr He. The inset in this plot shows the growth of $Fe(CO)_3DMB$ under the same conditions. (B) The formation of $Fe(CO)_3(DMB)_2$ monitored at 1986 cm^{-1}, generated by photolyzing 50 mTorr $Fe(CO)_5$ in the presence of 1.0 Torr DMB and 84Torr He. The absorbance units in both panels are arbitrary.

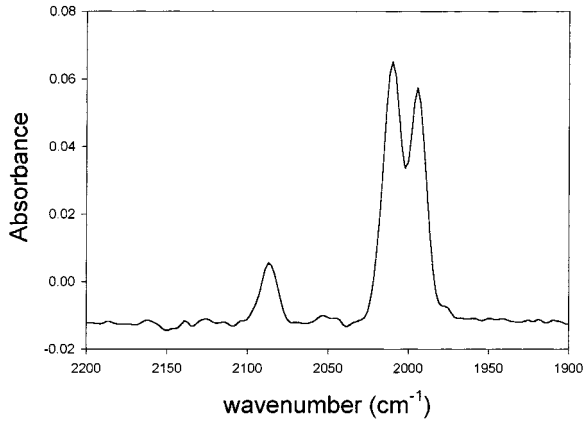

Figure 3. A gas-phase FT-IR spectrum of $Fe(CO)_4DMB$ obtained by subtracting the residual $Fe(CO)_5$ spectrum from the spectrum generated by 355-nm photolysis of a mixture of 100 mT $Fe(CO)_5$, 20 Torr DMB, and 80 Torr CO.

absorptions for $Fe(CO)_4DMB$ at 2094, 2012, and 1993 cm^{-1}. These predications match quite well with the absorptions at 2090, 2014, and 1995 cm^{-1} that are present in the spectrum in Figure 3. Assignment of these absorptions to $Fe(CO)_4DMB$ would imply that any $Fe(CO)_3(DMB)_2$ that is formed does not have a long enough lifetime to be observed on the time scale of the spectrum in Figure 3. This conclusion is verified by experiments performed in this study (vide infra) which directly determine the BDE and lifetime for $Fe(CO)_3(DMB)_2$. Therefore, the absorptions at 2090, 2014, and 1995 cm^{-1} in Figure 3 are assigned to $Fe(CO)_4DMB$.

TABLE 1: IR Absorptions of Relevant Iron Carbonyl Complexes of DMB and DMP[a]

complex	conditions	frequencies (cm^{-1})	ref
$Fe(CO)_3(DMP)$	3MP, 90 K	2041(1.0), 1966(1.1), 1953(1.2)	13
$Fe(CO)_3(DMB)$	gas, 297 K	2056, 1981, 1970	this work
$Fe(CO)_3(DMP)_2$	3MP, 90 K	2046(1.0), 1970(15)	13
$Fe(CO)_3(DMB)_2$	gas, 297 K	2060, 1986,1974	this work
$Fe(CO)_4DMP$	3MP, 298 K	2079(1.0), 1997(4.0), 1978(3.0)	13
$Fe(CO)_4DMB$	gas, 295 K	2090, 2014, and 1995	this work

[a] DMP= 3,3-dimethyl-1-pentene; 3MP= 3-methylpentene.

The absorptions for $Fe_2(CO)_8$, $Fe(CO)_3(DMB)$, $Fe(CO)_3(DMB)_2$, and $Fe(CO)_4DMB$, which are listed in Table 1, provide an explanation for all the features in the spectrum in Figure 1B. Both $Fe(CO)_3(DMB)$ and $Fe(CO)_3(DMB)_2$ absorb at ~2060, ~1986, and ~1970 cm^{-1}, and are present under conditions used to generate the data in Figure 1B. Moreover, $Fe_2(CO)_8$ has an absorption at ~2048 cm^{-1}.[12] Since all three of these species absorb in the 2045−2062 cm^{-1} region, the absorption in this region is broad. The absorption at ~2000 cm^{-1} may be due to $Fe(CO)_4DMB$ and/or a polynuclear species, probably $Fe_2(CO)_8DMB$. $Fe(CO)_4DMB$ could form by the reaction of $Fe(CO)_3DMB$ with CO that is produced by photolysis of $Fe(CO)_5$. Since the spectrum in Figure 1A was generated at a high enough DMB pressure that very little polynuclear species form, while the spectrum in Figure 1B was generated under conditions where significant polynuclear species form, polynuclear absorptions are expected to be present in spectrum 1C, which was generated by a scaled subtraction of 1A from 1B.

B. Addition Rate Constants. The rate constants for the relevant addition reactions were determined from plots of the rate of the addition process versus the pressure of the appropriate ligand (under pseudo-first-order conditions), monitored at an absorption of either or both the iron carbonyl reactant or the reaction product. Due to the convolution of the absorptions of $Fe(CO)_3(DMB)_2$ and $Fe(CO)_3(DMB)$, mentioned above, the probe frequencies were typically shifted a few wavenumbers from the peak of an absorption to monitor an edge of an $Fe(CO)_3(DMB)$ and/or $Fe(CO)_3(DMB)_2$ absorption band.

1. $Fe(CO)_3$ + DMB (k_1). The growth of $Fe(CO)_3DMB$ was monitored at 2071 cm^{-1} yielding a rate constant for reaction 1 of $(9.6 \pm 1.4) \times 10^{-11}$ cm^3 $molecule^{-1}$ s^{-1}. As indicated above, it was not possible to accurately monitor the decay of $Fe(CO)_3$.

2. $Fe(CO)_3DMB$ + DMB (k_2). The growth of $Fe(CO)_3(DMB)_2$ was monitored at 1986 cm^{-1}. As indicated above, the 1986 cm^{-1} absorption of $Fe(CO)_3(DMB)_2$ overlaps the $Fe(CO)_3DMB$ absorption in the region which is centered at 1981 cm^{-1}. However, only a rise was observed at 1986 cm^{-1}, implying that at this wavelength $Fe(CO)_3(DMB)_2$ is a stronger absorber than $Fe(CO)_3(DMB)$. Therefore, the rise rate of transient signal at this frequency can be used to monitor the rate of formation of $Fe(CO)_3(DMB)_2$. A typical signal is shown in Figure 2.B. The plot in Figure 4 of the rate for this process versus DMB pressure yields a rate constant of $(2.4 \pm 1.2) \times 10^{-12}$ cm^3 $molecule^{-1}$ s^{-1} at 24 °C. Within experimental error, this rate constant is temperature independent from 5 to 32 °C. The relatively large intercept in the plot in Figure 4 indicates that polynuclear species are also formed. The DMB dependence of the rate of decay of $Fe(CO)_3DMB$ was also monitored. When the DMB pressure was less than 0.5 Torr, the decay of $Fe(CO)_3DMB$ could be separated from the growth of $Fe(CO)_3(DMB)_2$ monitored at 2071 cm^{-1}. The rate constant of $(2.2 \pm 0.2) \times 10^{-12}$ cm^3 $molecule^{-1}$

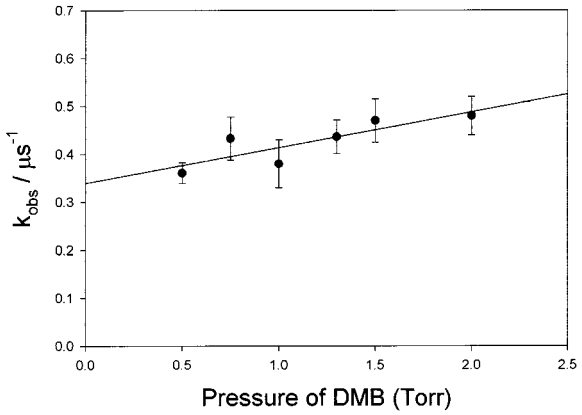

Figure 4. A plot of k_{obs} for the growth of $Fe(CO)_3(DMB)_2$ vs DMB pressure in the presence of 0.05 Torr $Fe(CO)_5$, monitored at 1986 cm^{-1}.

s^{-1}, obtained from the decay of $Fe(CO)_3DMB$, monitored at 2071 cm^{-1}, agrees well with the rate constant reported above that was obtained from the rise of $Fe(CO)_3(DMB)_2$. The average of the two values gives $(2.3 \pm 0.8) \times 10^{-12}$ cm^3 $molecule^{-1}$ s^{-1}.

3. $Fe(CO)_3DMB + CO$ (k_6). The CO dependence of the rise of $Fe(CO)_4DMB$, monitored at 2006 cm^{-1}, gave a value of $(4.2 \pm 0.4) \times 10^{-12}$ cm^3 $molecule^{-1}$ s^{-1} for k_6, the rate constant for the reaction in the title. The CO dependence of the decay of $Fe(CO)_3DMB$, monitored at 2071 cm^{-1}, gave a value of $(3.5 \pm 0.7) \times 10^{-12}$ cm^3 $molecule^{-1}$ s^{-1}, for k_6, which agrees well with the rate constant obtained at 2006 cm^{-1}. The average of these two measurements gives $k_6 = (3.9 \pm 0.6) \times 10^{-12}$ cm^3 $molecule^{-1}$ s^{-1}. Within experimental error this rate constant is temperature independent from 5 to 32 °C.

4. $Fe(CO)_3DMB + Fe(CO)_5$ (k_4). The rate constant for this reaction can be estimated from the intercept of the DMB pressure dependent plot of the decay rate of $Fe(CO)_3DMB$ monitored at 2071 cm^{-1}. For an $Fe(CO)_5$ concentration of 0.05 ± 0.01 Torr, the intercept of 29.3 ± 2.3 ms^{-1} leads to a rate constant for the reaction of parent with $Fe(CO)_3(DMB)$ of $\sim 2 \times 10^{-11}$ cm^3 $molecule^{-1}$ s^{-1}at 24 °C.

5. $Fe(CO)_4 + DMB$ (k'). The DMB dependence of the rate of the decay of $Fe(CO)_4$ monitored at 2001 cm^{-1} gave a rate constant for addition of DMB to $Fe(CO)_4$, k', of $(5.0 \pm 0.5) \times 10^{-13}$ cm^3 $molecule^{-1}$ s^{-1} at 24 °C. Due to the convolution of absorption bands, under the conditions and for times where $Fe(CO)_4DMB$ is produced in significant quantities, the only absorption that exhibited growth attributable to $Fe(CO)_4DMB$ was centered at 2090 cm^{-1}, and then only for low DMB pressures (<0.5 Torr) for a CO pressure of 5.5 Torr. When the DMB pressure is increased beyond ~0.5 Torr, the rate of the rising signal appeared to become slower. The observed growth rates are then smaller than the corresponding decay rates of $Fe(CO)_4$ monitored at 2001 cm^{-1}. Simulations via Chemical Kinetics Simulator software[16] show that increasing the DMB pressure results in the formation of more $Fe(CO)_3(DMB)$ and $Fe(CO)_3(DMB)_2$. The decay of $Fe(CO)_3(DMB)$ and the growth of $Fe(CO)_4(DMB)$ are then convoluted, making the formation of $Fe(CO)_4(DMB)$ *appear* slower. The other two absorptions of $Fe(CO)_4DMB$, centered at 1995 and 2014 cm^{-1}, were also investigated. The signal at 1995 cm^{-1} decays to a plateau whose amplitude increases relative to the amplitude of the decay as the pressure of DMB is increased. At 2014 cm^{-1}, a decay that goes below the baseline was obtained, which is due to the convolution of the absorption of $Fe(CO)_4DMB$ with the very strong absorption of $Fe(CO)_5$. These convolutions preclude measuring k' at these frequencies and 2001 cm^{-1} is the only frequency that was used to determine k'. Within experimental error, k' is temperature independent over 5−32.5 °C.

C. $Fe(CO)_3(DMB)$−DMB Bond Dissociation Energy. The kinetic scheme used to determine the bond dissociation energy of $Fe(CO)_3(DMB)_2$ is based on one that has been used to determine BDEs for dissociative loss of a variety of ligands bound to metal carbonyls.[5,9] Dissociative loss is expected for weakly bound ligands, especially when "slippage" of an already bound ligand, which could result in opening up a coordination site, is not possible. Without ligand slippage, a reaction involving an associative ligand substitution process would require a 6-coordinate intermediate that is a greater than an 18 electron species. Such a process would be expected to involve a significant activation energy.

The relevant reactions for this mechanism are

$$Fe(CO)_3(DMB)_2 \xrightarrow{k_d} Fe(CO)_3DMB + DMB \quad (5)$$

$$Fe(CO)_3DMB + DMB \xrightarrow{k_2} Fe(CO)_3(DMB)_2 \quad (2)$$

$$Fe(CO)_3DMB + Fe(CO)_5 \xrightarrow{k_4} Fe_2(CO)_8DMB \quad (4)$$

$$Fe(CO)_3DMB + CO \xrightarrow{k_6} Fe(CO)_4(DMB) \quad (6)$$

Applying the steady-state approximation to $Fe(CO)_3DMB$ results in the following expression involving the rate constant, k_d, for dissociation of $Fe(CO)_3(DMB)_2$:

$$k_{obs} = \frac{k_d(k_6[CO] + k_4[Fe(CO)_5])}{k_2[DMB] + k_6[CO] + k_4[Fe(CO)_5]} \quad (7)$$

k_{obs} is the phenomenological rate constant for the disappearance of $Fe(CO)_3(DMB)_2$. This process has been probed at both 1986 and 1974 cm^{-1}. On the millisecond time scale the decay of the $Fe(CO)_3(DMB)_2$ at 1986 cm^{-1} did not reach the baseline. This behavior may be due to an underlying absorption of $Fe(CO)_4$-(DMB) centered at 1995 cm^{-1}. However, the decay at 1974 cm^{-1} goes to the baseline and the signals obtained at this wavelength have the same behavior, as a function of DMB and CO pressure, as observed at 1986 cm^{-1}. Thus, the disappearance of the $Fe(CO)_3(DMB)_2$ was systematically monitored at 1974 cm^{-1}.

By varying the DMB and CO pressures, k_d can be calculated. From eq 7 it is clear that if the pressure of DMB and CO are high enough, $k_4[Fe(CO)_5]$ will be negligible relative to the other terms in the denominator and, within experimental error, k_{obs} will depend on the [DMB]/[CO] ratio rather than the individual DMB and CO pressures. Under these circumstances, neglecting the term, $k_4[Fe(CO)_5]$, eq 7 can be rewritten as

$$\frac{1}{k_{obs}} = \left(1 + \frac{k_2}{k_6} \times \frac{[DMB]}{[CO]}\right) \times \frac{1}{k_d} \quad (8)$$

For these conditions: 0.050 Torr $Fe(CO)_5$, 10 to ~150 Torr DMB, and 5.3 to ~31 Torr CO, k_{obs} will depend on [DMB]/[CO] ratio, and as seen in Figure 5A, a plot of $(1/k_{obs})$ versus the DMB]/[CO] ratio gives a straight line. The linearity of this plot indicates that the experimental data is consistent with the kinetic scheme consisting of eqs 2,4,5, and 6. Additionally, as expected, the yield of $Fe(CO)_3(DMB)_2$ increased with increasing DMB pressure and *decreased* with increasing CO pressure. Thus, the minimum DMB/CO ratio that was used in these experiments was effectively determined by the DMB/CO ratio

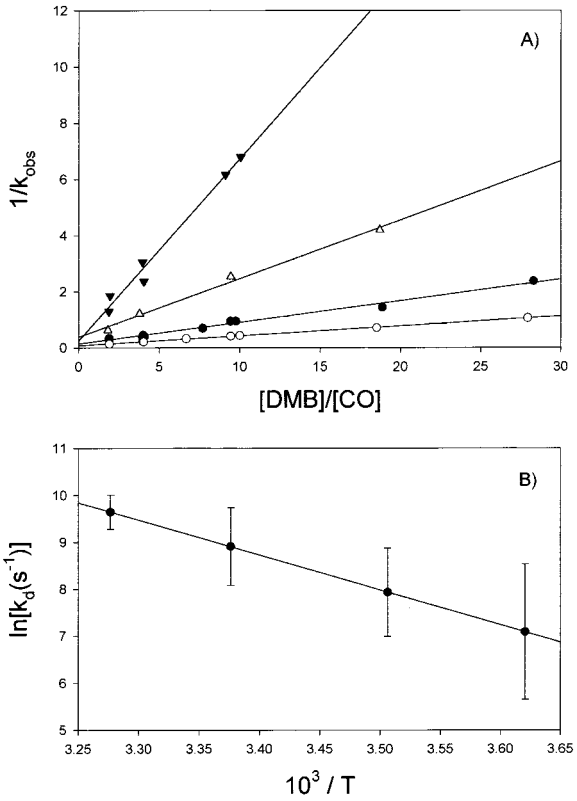

Figure 5. (A) A plot of $(1/k_{obs})$ vs [DMB]/[CO], where k_{obs} is for the decay of $Fe(CO)_3(DMB)_2$ at 1974 cm^{-1} in the presence of 50 mTorr Torr $Fe(CO)_5$: at 280 K(▼), 285 K (△), 296 K (●), and 305 K(○), respectively. The units on the ordinate are ms. (B) An Arrhenius plot for the loss of DMB from $Fe(CO)_3(DMB)_2$. The rate constant for dissociative loss of DMB, k_d, is plotted versus $10^3/T$.

necessary to produce a transient for the decay of $Fe(CO)_3(DMB)_2$ that has an acceptable signal-to-noise level.

Since k_2 and k_6 have been measured and are temperature independent, the temperature dependence of k_d can be determined directly from k_{obs}, which can then be related to the bond dissociation enthalpy. In this case using eq 8, a value for k_d was computed for each value of k_{obs}, at each temperature, and the average value is reported. An Arrhenius plot of ln k_d vs $10^3/T$ for $Fe(CO)_3(DMB)_2$ is shown in Figure 5B. From these data the bond enthalpy for the process reaction 5

$$Fe(CO)_3(DMB)_2 \xrightarrow{k_d} Fe(CO)_3DMB + DMB \qquad (5)$$

can be calculated as 15.2 ± 3.8 kcal mol^{-1}, and the intercept of the plot gives ln $A = 34.0 \pm 2.2$.

The error limits on the bond enthalpy were calculated using a propagation of errors analysis based on the errors in the k_d for each temperature. It is interesting to note that the value for ln A cited above is very similar to the values of ln A obtained for loss of pentene and ethylene from $Fe(CO)_3(olefin)_2$, which are 36.2 and 33, respectively.[8] Ligand loss processes of this type are anticipated to involve a change in spin from a singlet $Fe(CO)_3L_2$ complex to a triplet $Fe(CO)_3L$ species. Entropies of activation for some reactions of this type and for the relevant reverse reactions are discussed in ref 8 in the context of the expected change in spin that takes place during the reaction.

D. $Fe(CO)_4(DMB)$ Dissociation. $Fe(CO)_4(DMB)$ was monitored at 1995 cm^{-1} and 2014 cm^{-1} using the FTIR. At these wavelengths the signal decayed to a nonzero value and became slower when the CO pressure was increased from 10 Torr ($\sim$0.28 min^{-1}) to 80 Torr ($\sim$0.14 min^{-1}). However, there was no apparent trend in the rate of decay as the DMB/CO ratio was varied. When the temperature was increased to 35 °C, the decay rate was larger ($\sim$0.25 min^{-1} for 80 Torr CO, and $\sim$0.6 min^{-1} for 10 Torr CO).

TABLE 2: Summary of Rate Constants for Addition Reactions Involving $Fe(CO)_3$, $Fe(CO)L$, and $Fe(CO)_4$ Species[a]

reaction	rate constant (cm^3 $molecule^{-1}$ s^{-1})	spin conserving?
$Fe(CO)_3 + C_2H_4$[15]	$(2.2\pm 0.2) \times 10^{-10}$	Yes
$Fe(CO)_3 + C_2F_4$[9]	$(3.3\pm 1.2) \times 10^{-11}$	Yes
$Fe(CO)_3 + C_2Cl_4$[28]	$(3.0\pm 0.8) \times 10^{-11}$	Yes
$Fe(CO)_3$ + DMB	$(9.6 \pm 1.4) \times 10^{-11}$	Yes
$Fe(CO)_3$ + PD[29]	$(2.8 \pm 0.3) \times 10^{-10}$	Yes
$Fe(CO)_3$ + propene[7]	$(2.6 \pm 0.3) \times 10^{-10}$	Yes
$Fe(CO)_3$ + 1-pentene[8]	$(4 \pm 1) \times 10^{-10}$	Yes
$Fe(CO)_3(C_2H_4) + C_2H_4$[15]	$(1.1\pm 0.3) \times 10^{-11}$	No
$Fe(CO)_3(C_2H_4)$ + propene[7]	$(1.8\pm 0.3) \times 10^{-11}$	No
$Fe(CO)_3(C_2F_4) + C_2F_4$[9]	$(5.4\pm 1.7) \times 10^{-12}$	No
$Fe(CO)_3(C_2Cl_4) + C_2Cl_4$[28]	$(1.9\pm 0.3) \times 10^{-13}$	No
$Fe(CO)_3(DMB)$ + DMB	$(2.3 \pm 0.8) \times 10^{-12}$	No
$Fe(CO)_3(C_2H_4) + CO$[15]	$(4.3\pm 0.8) \times 10^{-12}$	No
$Fe(CO)_3(C_2Cl_4) + CO$[28]	$(2.4\pm 0.6) \times 10^{-12}$	No
$Fe(CO)_3(DMB) + CO$	$(3.9\pm 0.6) \times 10^{-12}$	No
$Fe(CO)_4 + C_2H_4$[9]	$(1.7\pm 0.2) \times 10^{-13}$	No
$Fe(CO)_4 + C_2F_4$[9]	$(1.3\pm 0.5) \times 10^{-14}$	No
$Fe(CO)_4 + C_2Cl_4$[28]	$(1.2\pm 0.3) \times 10^{-13}$	No
$Fe(CO)_4$ + DMB	$(5.0\pm 0.5) \times 10^{-13}$	No
$Fe(CO)_4$ + 1,3-PD[29]	$(1.2\pm 0.1) \times 10^{-12}$	No
$Fe(CO)_4$ + 1,4-PD[29]	$(5.8\pm 0.3) \times 10^{-13}$	No
$Fe(CO)_3(C_2H_4) + Fe(CO)_5$[9]	$(4\pm 2) \times 10^{-11}$	
$Fe(CO)_3(C_2Cl_4) + Fe(CO)_5$[28]	$(9.7\pm 3.5) \times 10^{-12}$	
$Fe(CO)_3(DMB) + Fe(CO)_5$	$\sim 2 \times 10^{-11}$	

[a] PD, pentadiene. Where a reference is not indicated, the data is from this work.

IV. Discussion

A. Comparisons among Rate Constants for Reactions of the Type: $Fe(CO)_3 + L$, $Fe(CO)_3L + L$, and $Fe(CO)_4 + L$ ($L = C_2H_2$, C_2Cl_4, C_2F_4, and DMB). The rate constants for the addition reaction of L to both $Fe(CO)_3$ and $Fe(CO)_3(L)$ are listed in Table 2. The rate constants for reaction of $Fe(CO)_3$ with perhalogenated olefins are smaller than those for reaction with unsubstituted linear olefins, with DMB lying almost between those for the halogenated and unsubstituted linear olefins. As expected, the reactions of $Fe(CO)_3 + L$ are much faster than the reactions of $Fe(CO)_3L + L$ [5,17] and $Fe(CO)_4 + L$. Since $Fe(CO)_4$ has a triplet ground state and $Fe(CO)_3L$ species are anticipated to have triplet ground states,[17] reactions of this type are expected to be spin-disallowed and an intersystem crossing must occur to yield stable singlet products.[5] If crossing from the triplet to the singlet potential energy surface is rate limiting, then factors that influence the probability for this process will affect the magnitude of the relevant rate constant-(s). Clearly, the specifics of the nature of the states involved and the details of the shape of the intersection for these potential surfaces could have a significant effect on the rate of curve crossing and thus the rate constant for a reaction. However, it is very difficult to obtain accurate information regarding these issues. As such, we will consider whether properties of ligands, which could also effect the probability of curve crossing, such polarizability and ligand size and shape (steric effects) correlate with the magnitude of the relevant rate constants.[5,17]

One factor that has been previously considered is the polarizability of the entering ligand.[17] Since a curve crossing must occur to produce stable products, a complex that has a longer lifetime on the triplet potential surface will, with all else

TABLE 3: BDEs of $Fe(CO)_3(olefin)_2$ Complexes

	$Fe(CO)_3(C_2H_4)_2$	$Fe(CO)_3(C_2Cl_4)_2$	$Fe(CO)_3(C_2F_4)_2$	$Fe(CO)_3(DMB)_2$	$Fe(CO)_3(\eta^2\text{-pentene})_2$
BDE/kcal mol^{-1}	21.3 ± 2.0[9]	≥ 22[28]	≥ 22[9]	15.2 ± 3.8[a]	20.2 ± 0.7[8]

[a] This work.

TABLE 4: The Average Electric Dipolar Polarizabilities for the Ground States of Relevant Ligands

ligand	CO	C_2Cl_4	C_2F_4	C_2H_4	propene	*trans*-1,3-PD	1-pentene	2,3-dimethyl-1-butene
polarizability (10^{-24} cm^3)	1.95	17.6[a]	6.3[a]	4.26	6.26	10.0	9.65	11.8

[a] Calculated by a DFT method,[27] the others are from ref 18.

being equal, have a higher probability for curve crossing. A more polarizable ligand would be expected to lead to a deeper well, and potentially a longer lifetime for a triplet complex. The average electric dipolar polarizabilities for the ground states of relevant ligands are listed in Table 4. When available, polarizabilites were taken from the *Handbook of Chemistry and Physics*.[18] The polarizability of 3,3-dimethyl-1-butene was not available. As such, the assumption was made that it was not significantly different than the polarizability for 2,3-dimethyl-1-butene, which is known. The electric dipolar polarizabilities of C_2Cl_4 and C_2F_4 were calculated using a density function theory (DFT) method.[19] There are some interesting observations that can be made based on the data in this Table. For example, 1,3-pentadiene has the largest polarizability of the ligands studied, and the largest rate constant for reaction with $Fe(CO)_4$. However, considering only polarizability, it is not obvious why the reaction of $Fe(CO)_3C_2H_4 + C_2H_4$ is faster than the reaction of $Fe(CO)_3DMB + DMB$.

Another factor that can affect the magnitude of the rate constant for a ligand addition process is ligand size. A common term used to refer to the effect of ligand size is the "steric effect". However, it should be realized that both the size and shape of a ligand can effect its interaction with a coordinatively unsaturated metal carbonyl. A "large" ligand could also lead to a minimum in the triplet potential surface at larger distances than occurs with a "smaller" ligand. This could make accessing the curve crossing less probable and could even lead to a barrier for curve crossing. These issues have been discussed in more detail in refs 5 and 17. Large ligands and those with less than optimal shape for efficient overlap of bonding orbitals may also lead to weaker bonding. Tolman's cone angle,[20] solid angles,[21] and Brown's ligand repulsive energy, E_R,[22] which is calculated based on a static force field, are three popular quantitative measures of the steric effect of a ligand.[23] However, for ligands that depart significantly from cylindrical symmetry about the M−L bond axis, both the two-dimensional cone angle or the solid cone angle is less clearly related to the effective volume in space the ligand subtends. For example, the shapes of η^2-coordinated olefins are sufficiently far removed from conical to render the cone angle methodology ineffective as a measure of alkene size.[24] The ligand repulsive energy parameter, E_R, defined in terms of the change in the van der Waals repulsive energy with distance, or an analogue of this parameter would be expected to be a more reasonable measure of steric interactions.[24,25]

In this work we employ a semiquantitative measure of the effect of the size and shape of a ligand on bonding interactions. The steric repulsive energy, which is qualitatively similar to E_R, was calculated using the Tripos force field, available in the Sybyl molecular mechanics program.[26] The steric repulsive energy is the magnitude of the repulsive interaction when a ligand approaches an unsaturated $Fe(CO)_3(L)$ fragment. (In all cases the approaching olefin was the same chemical species as the bound olefin.) The steric interaction energies were calculated by restricting the approach of the free olefin to the $Fe(CO)_3L$ moiety in an orientation and direction that would lead to an optimized bonding geometry, as calculated using DFT.[27] The distance at which the interaction energy was calculated was 0.2 Å greater than the equilibrium bonding distance of the olefin to the $Fe(CO)_3L$, again as calculated using DFT.[27] At this distance the geometry, as calculated using DFT, could be maintained for all systems and a steric interaction energy could be calculated for the constrained geometry.

Both the results obtained from Sybyl and the E_R values for olefins bound to $Cr(CO)_5$, calculated by White and Brown,[25] show that DMB has a larger steric interaction with the relevant unsaturated complex than either ethene or 1-propene. The implication being that the relatively high degree of steric interaction could be at least a factor in the relatively small rate constant for the reaction of $Fe(CO)_3DMB + DMB$. Interestingly, results from Sybyl also indicate that the large substituents around the double bond in C_2Cl_4 lead to a larger steric interaction for it approaching $Fe(CO)_3(C_2Cl_4)$ than for DMB approaching $Fe(CO)_3DMB$.[28] The methyl and methylene groups in DMB can "fold back" away from the $Fe(CO)_3DMB$ to minimize the steric interaction energy. Though there is no experimental evidence for formation of a stable iron carbonyl bis olefin complex with 1,3-PD or 1,4-PD,[29] the interaction energies with these ligands can still be evaluated. As anticipated, these species have modest interaction energies (~50% of the value for DMB and ~50% more than the value for ethylene) since the methyl and methylene groups can "fold back" away from the other ligands in the $Fe(CO)_3(PD)$ complex. As might be expected, the steric repulsive contribution to the overall energy for tetrachloroethylene is also much larger than for both ethylene and tetrafluoroethylene.

A plot of the rate constants for these addition reactions versus the relative steric interaction energy for L approaching $Fe(CO)_3L$ is shown in Figure 6A. Interestingly, an increase in the magnitude of the steric interaction energy correlates with smaller rate constants. Similarly, White and Brown found that the second-order rate constant for the coordination of olefins to $HCo[PPh(Oet)_2]_3$ gets smaller as the interaction energy goes up.[25] However, a more dramatic correlation can be established between rate constant and steric interaction energy if a plot is made of the log of the rate constant versus the steric interaction energy divided by the polarizability of L. Though a significant linear correlation is apparent in this plot, we do not take this correlation, by itself, to be indicative of a specific fundamental relationship between the rate constant and the quotient of terms that is plotted. Rather we take it as an interesting empirical relationship. Clearly it is plausible that a larger polarizability tends to give a larger rate constant and a larger steric interaction energy tends to give a smaller rate constant. Intuitively, one would expect that for sufficiently small steric terms, the specific magnitude of the steric interaction energy will no longer be a

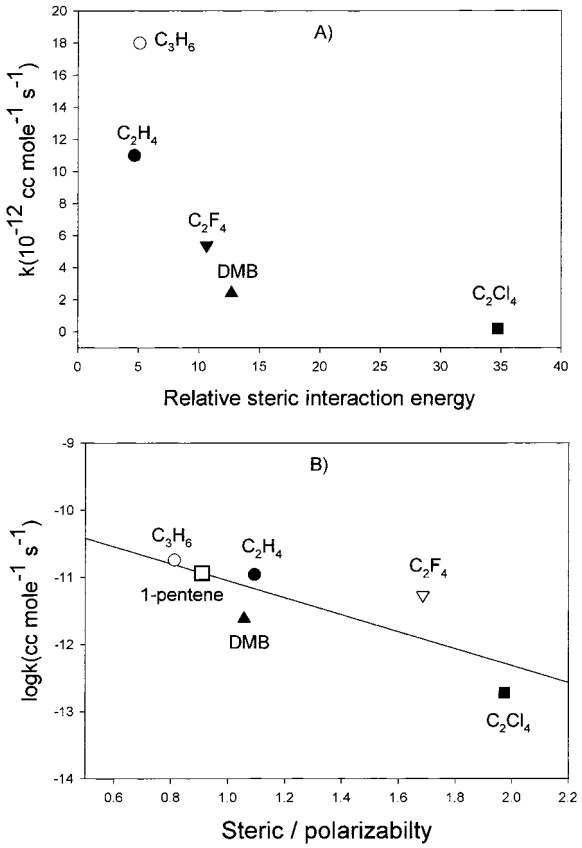

Figure 6. (A) A plot of addition rate constants for the reaction of $Fe(CO)_3L + L$ versus the relative steric interaction energy. (B) A plot of the log of the addition rate constants for $Fe(CO)_3L + L$ versus the ratio of the steric interaction energy and the polarizability. The polarizability is in units of 10^{-24} cm^3 while the steric interaction energy is in arbitrary units. The rate constant for $Fe(CO)_3(C_2H_4) + C_3H_6$ was taken to be the same as the rate constant for the reaction of $Fe(CO)_3(C_3H_6) + C_3H_6$. Note: the calculated result for $Fe(CO)_3$(1-pentene) + 1-pentene is shown as □.

controlling factor. It is interesting to note that an extrapolation to zero steric interaction energy predicts a rate constant of $\sim 2 \times 10^{-10}$ cm^3 molecule^{-1} s^{-1}, which is larger by more than an order of magnitude than the largest rate constants we have measured for the addition of any ligand to an $Fe(CO)_3L$ species.

The correlations implied by the plot are certainly interesting and clearly deserve to be tested for other systems. If this correlation stands up to further testing it could potentially be used to predict rate constants for the appropriate class(es) of reactions. This type of correlation is analogous to many linear free energy relationships in which the log of the rate constant is plotted versus a relevant parameter(s).[30] One such relationship is the Taft equation in which the linear free energy relationship for the rate constant for the reaction of aliphatic esters correlates with both steric and electronic factors.[31]

Interestingly, based on this plot, since the ratio of the steric interaction energy/ polarizability is about 1.1 for 1-pentene, the rate constant for the reaction of $Fe(CO)_3$(1-pentene) + 1-pentene is predicted to be $\sim 1.2 \times 10^{-11}$ cm^3 molecule^{-1} s^{-1}. This value lies between the rate constant for reaction of $Fe(CO)_3DMB$ + DMB and the rate constant for reaction of $Fe(CO)_3(C_2H_4)$ + C_2H_4, and somewhat closer to the rate constant for the latter reaction.

B. Comparison of $Fe(CO)_3L-L$ Bond Dissociation Enthalpies ($L = C_2H_2$, C_2Cl_4, C_2F_4, and DMB). The BDEs that have been measured for $Fe(CO)_3(L)_2$ complexes, where L is an olefin, are listed in Table 3. Details of the factors that can effect bonding in bis-olefin complexes of transition metals have been discussed in refs 1 and 32−34. The expected geometry of the bis olefin complexes is one in which the olefins occupy equatorial sites. This geometry is consistent with the fact that the same pattern of absorptions is observed for all of the bis-olefin complexes of iron that are indicated in Table 3, and it has been confirmed by calculations of the lowest energy geometry of these complexes.[27] For such a geometry the olefins compete with each other and a CO group for electron density. Thus, with everything else being equal, a better π acceptor is likely to form a stronger bond with the metal center and a better σ donor will also bond more strongly. The bulkier the ligand, the more steric hindrance there will be in the approach of the ligand to its optimal bonding geometry. Such steric interactions can decrease the overall bond energy as a result of an increase in the deformation energy necessary to achieve an optimal bonding geometry,[35] and it may be more difficult for a ligand and a metal center to achieve optimal orbital overlap. The most straightforward comparison that can shed light on the principal determining factor as to the source of the difference in BDE for the bis-DMB complex versus the other bis-olefin complexes in Table 3 is with 1-pentene. The energy of the $\pi-\pi^*$ transitions in linear olefins does not change significantly in going from butene to hexene ($\sim$0.1 eV).[32] Similarly, the energy of this transition is only 0.02 eV different for 1-hexene versus 2-methyl-1-pentene.[32] Thus, the principal difference in the electron-accepting and -donating abilities of 1-pentene versus DMB would be expected to result from the additional carbon centered moiety in the DMB framework. This should lead to DMB being a slightly better electron donor than 1-pentene. This prediction is consistent with the small shift toward lower frequency for the carbonyl stretching absorptions of the bis-DMB complex relative to the bis-(1-pentene) complex. *However, the BDE decreases in going from the bis-1-pentene complex to the bis-DMB complex*. This clearly points to other determining factors for the BDEs in these systems. The most obvious is the larger bulk and concomitantly greater steric interaction energy for the bis-DMB complex. As such, we conclude that the smaller BDE for the bis-DMB complex is correlated with the greater steric interactions in this complex. This conclusion is consistent with the expectation that the BDE for $Fe(CO)_3(olefin)_2$ decreases as the size of the olefin increases.[1,32] However, we again point out that the number of carbons in the olefin is not, in itself, expected to be as significant as the magnitude of the steric interaction energy which is influenced by the geometry of the olefin, particularly in the vicinity of the double bond.

C. Dissociation of $Fe(CO)_4DMB$. The decay of $Fe(CO)_4$-DMB occurs on a time scale of minutes. As such, this complex is much more stable than $Fe(CO)_3(DMB)_2$. The same trend in stability has been observed for most other olefins: the mono-substituted compounds are more stable than the disubstituted compounds.[9,28] A notable exception to this is for C_2F_4 where $Fe(CO)_3(C_2F_4)_2$ may have a BDE that is similar to that for $Fe(CO)_4C_2F_4$. This system is discussed in more detail in ref 9.

Under experimental conditions, even when the reaction is carried out in the presence of only 10 Torr of CO, the measured value for k_{obs} would be expected to be close to k_d. Although only two temperature measurements were made, the values obtained for the E_a, of $\sim$8.7 kcal/mol and the ln A, of $\sim$8.8 for the rate of loss of $Fe(CO)_4DMB$ are sufficiently small to indicate that what is occurring is not a simple homogeneous gas-phase process leading to ligand loss. This is true whether $Fe(CO)_4DMB$ loses DMB, as would be anticipated, or if it were to decompose by CO loss. Such small values for the preexpo-

nential factor and the activation energy for the reaction suggest that the decay of $Fe(CO)_4DMB$ involves a multiple step pathway and/or heterogeneous process taking place on the cell walls.[9] The latter possibility is bolstered by the fact that similar behavior observed for $Fe(CO)_4L$ ($L = C_2H_4$, C_2Cl_4, and C_2F_4) has been attributed to such processes.[9,28] Additionally, $Fe(CO)_4DMP$ is sufficiently stable at room temperature that an IR spectrum of the species has been obtained using standard techniques.[13] Thus, we believe that available evidence points to decay of $Fe(CO)_4DMB$ via heterogeneous processes taking place on the cell walls.

D. Thermochemistry of the Isomerization of 1-Pentene. As described in Section I, to date, it has not proven possible to directly measure the addition rate constant, k_+, (in eq 10) when an olefin contains allylic hydrogens, since in the systems that have been investigated in detail, a very rapid β-hydrogen transfer process takes place following what has been the rate-limiting addition of an olefin to $Fe(CO)_3$.[7,8] However, the magnitude of k_+ is central to the calculation of thermodynamic parameters involved in the mechanism for olefin isomerization. For example, in previous studies of the mechanism of olefin isomerization of 1-pentene, the equilibrium constants for the equilibria in eqs 9 and 10 were calculated using eqs 11 and 12, respectively:[8]

$$Fe(CO)_3(\eta^2\text{-1-pentene}) \underset{k'_-}{\overset{k'_+}{\rightleftharpoons}} HFe(CO)_3(\eta^3\text{-}C_5H_9) \quad (9)$$

$$Fe(CO)_3(\eta^2\text{-1-pentene}) + \text{1-pentene} \underset{k_-}{\overset{k_+}{\rightleftharpoons}} Fe(CO)_3(\eta^2\text{-1-pentene})_2 \quad (10)$$

$$K'_{eq} = \frac{\frac{(1-\%)k_-}{\%}}{k_+[1-pentene]} \quad (11)$$

$$K_{eq} = \frac{k_+}{k_-} \quad (12)$$

The percent (%) symbol refers to the percentage of initially formed $HFe(CO)_3(\eta^3\text{-}C_5H_9)$ that remains after an equilibrium is established between $HFe(CO)_3(\eta^3\text{-}C_5H_9)$ and $Fe(CO)_3(\eta^2\text{-1-pentene})_2$. Since k_+ could not be directly measured, it was estimated on the basis of the average of the rate constants for the reaction of $Fe(CO)_3(C_2H_4) + C_2H_4$, and the reaction of $Fe(CO)_3(C_2H_4) + C_3H_6$.[7,8] These are both systems in which β-hydrogen transfer does not take place since ethylene does not have β-hydrogens. However, clearly it would be more appropriate and accurate to use the rate constant for addition of 1-pentene to $Fe(CO)_3$(1-pentene). This rate constant has been estimated in Section IV.A as 1.2×10^{-11} cm^3 molecule^{-1} s^{-1}. As would be expected, the magnitude for this rate constant is bracketed by the values that have been experimentally determined for the addition of ethylene and DMB to their respective $Fe(CO)_3$(olefin) complexes.

Using eq 11 obtained from ref 8, the equilibrium constant, K'_{eq} for the equilibrium between $Fe(CO)_3(\eta^2$-1-pentene) and $HFe(CO)_3(\eta^3\text{-}C_5H_9)$ is calculated to be 3.2×10^{-8}. Using the standard relation

$$\Delta G' = -RT \ln K'_{eq}$$

$\Delta G'$ is calculated to be $\sim$10.2 kcal mol^{-1} at the standard ambient temperature of 298 K and a pressure of 1bar (SATP). In addition, ΔG for the equilibrium between $Fe(CO)_3(\eta^2$-1-pentene) and $Fe(CO)_3(\eta^2$-1-pentene)$_2$ is calculated to be ~ -9.8 kcal mol^{-1}. These values can then be compared with the previous corresponding results, of $\sim$10.5 kcal mol^{-1}and ~ -9.9 kcal mol^{-1}, respectively, which were based on $k_+ = 6 \times 10^5$ s^{-1} T^{-1}. Thus, there is no more than an $\sim$0.3 kcal mol^{-1} difference between the two sets of results, which is less than the experimental error limits. This indicates that though there are differences in the magnitude of k_+ as estimated in this study versus the value used in prior work, the difference between the rate constants for the association reactions of $Fe(CO)_3(C_2H_4) + C_2H_4$ and $Fe(CO)_3$(1-pentene) + 1-pentene (estimated on the basis of the correlation in Figure 6) do not produce significant differences in the thermochemical parameters relevant in the isomerization of 1-pentene.

V. Conclusions

The infrared absorptions of $Fe(CO)_3DMB$, $Fe(CO)_3(DMB)_2$, and $Fe(CO)_4DMB$ have been observed. By probing the absorptions of reactants and/or products, bimolecular rate constants for the reactions of $Fe(CO)_3$ + DMB, $Fe(CO)_3DMB$ + DMB, $Fe(CO)_4$ + DMB, and $Fe(CO)_3DMB$ + CO have been measured as $(9.6 \pm 1.4) \times 10^{-11}$, $(2.3 \pm 0.8) \times 10^{-12}$, $(5.0 \pm 0.5) \times 10^{-13}$, and $(3.9 \pm 0.6) \times 10^{-12}$ cm^3 molecule^{-1} s^{-1}, respectively. The bond dissociation enthalpy for loss of DMB from $Fe(CO)_3(DMB)_2$ has been determined as 15.2 ± 3.8 kcal mol^{-1}. This value is smaller than values obtained in prior studies of the dissociation of other $Fe(CO)_3(L)_2$ complexes, where L is a smaller olefin, and is compatible with the larger steric interaction energy calculated for DMB interacting with $Fe(CO)_3$(DMB) relative to L interacting with $Fe(CO)_3L$. Data indicate that there is a correlation between the log of the rate constant for addition of an olefin L to $Fe(CO)_3L$ and the steric interaction energy for L interacting with $Fe(CO)_3L$ divided by the polarizability of L.

Thermochemical parameters relevant to the isomerization of 1-penetene, which were calculated on the basis of the association reactions of $Fe(CO)_3(C_2H_4) + C_2H_4$, do not change significantly when recalculated using the new estimate of the rate constant for addition of 1-pentene to $Fe(CO)_3$(pentene), which is based on data in Figure 6B, which correlates the rate constants for ligand addition processes with the ratio of the steric interaction energy divided by the ligand polarizability.

Acknowledgment. We acknowledge support of this work by the National Science Foundation under Grant NSF 97-34891. We also thank Dr. David Cedeño for calculating the expected equilibrium geometries of relevant $Fe(CO)_3L$ and $Fe(CO)_3L_2$ complexes and the polarizabilities for C_2Cl_4 and C_2F_4.

References and Notes

(1) Collman, J. P.; Hegedus, L. S.; Norton, J. R. *Principles and Applications of Organotransition Metal Chemistry*; University Science Books: Mill Valley, CA, 1987.

(2) Pearson, A. J. *Iron Compounds in Organic Synthesis*; Academic Press: London, 1994.

(3) Jordan, R. B. *Reaction Mechanisms of Inorganic and Organometallic Systems*; Oxford University Press: New York, 1991.

(4) Crabtree, R. H. *The Organometallic Chemistry of the Transition Metals*; Wiley-Interscience: New York, 1994.

(5) Weitz, E. *J. Phys. Chem.* **1994**, *98*, 11256.

(6) Weitz, E. *J. Phys. Chem.* **1987**, *91*, 3945.

(7) Long, G. T.; Wang, W.; Weitz, E. *J. Am. Chem. Soc.* **1995**, *117*, 12810.

(8) Long, G. T.; Weitz, E. *J. Am. Chem. Soc.* **2000**, *117*, 12810.

(9) House, P. G.; Weitz, E. *J. Phys. Chem.* A **1997**, *101*, 2988.

(10) Ryther, R. J.; Weitz, E. *J. Phys. Chem.* **1991**, *95*, 9841.

(11) Rayner, D. M.; Ishikawa, Y.-I.; Brown, C. E.; Hackett, P. A. *Laser Chemistry of Organometallics*; Chaiken, J., Ed.; ACS Symp. Ser., No. 530, American Chemical Society: Washington, DC, 1993.
(12) Ryther, R. J.; Weitz, E. *J. Phys. Chem*. **1992**, *96*, 2561.
(13) Wuu, Y. M.; Bentsen, J. G.; Brinkley, C. G.; Wrighton, M. S. *Inorg. Chem.* **1987**, 26, 530.
(14) Weiller, B. H.; Miller, M. E.; Grant, E. R. *J. Am. Chem. Soc*. **1987**, *109*, 352.
(15) Hayes, D. M.; Weitz, E. *J. Phys. Chem*. **1991**, *95*, 2723.
(16) *Chemical Kinetics Simulations*, Version 1.0.1 for Windows; IBM Research Corp.
(17) House, P. G.; Weitz, E. *Chem. Phys. Lett*. **1997**, *266*, 239.
(18) Handbook of Chemistry and Physics, 80th ed.; Lide, D. R., Ed.; CRC Press: Boca Raton, FL, 1999−2000.
(19) Jaguar 4.0, Schrodinger, Inc., Portland, OR, 1998−1999.
(20) Tolman, C. A. *J. Am. Chem. Soc*. **1970**, *92*, 2953.
(21) White, D.; Taverner, B. C.; Leach, P. G. L.; Coville, N. J. *J. Comput. Chem*. **1993**, *14*, 1042.
(22) Brown, C. A. *Chem. Rev*. **1977**, *77*, 313.
(23) Brown, T. L.; Lee, K. J. *Coord. Chem. Rev*. **1993**, *128*, 89.
(24) Bubel, R. J.; Douglass, W.; White, D. P. *J. Comput. Chem*. **2000**, *21*, 239.
(25) White, D. P.; Brown, T. L. *Inorg. Chem*. **1995**, *34*, 2718.
(26) Sybyl version 6.6, Tripos Inc., 1999.
(27) Cedeno, D. L; Weitz, E. Unpublished results
(28) Cedeno, D. L.; Weitz, E. *J. Phys. Chem*. A **2000**, *104*, 8011.
(29) Gravelle, S. J.; van de Burgt, L. J.; Weitz, E. *J. Phys. Chem*. **1993**, *97*, 5272.
(30) Gillion, R. D. *Introduction to Physical Organic Chemistry*; Addision-Wesley: Reading, MA, 1970; pp 156−160.
(31) Ananada, S.; Jagadeesha, M. B.; Puttaswamy, Venkatesha B. M.; Vinnod, T. K.; Gowda, N. M. M. *Int. J. Chem. Kinet*. **2000**, *32*, 776.
(32) Pruchnik, F. P. *Organometallic Chemistry of the Transition Elements*; Plenium Press: New York, 1990.
(33) Wick, D. D.; Jones, W. D. *Organometallics* **1999**, *18*, 495.
(34) Halpern, J. *Inorg. Chim. Acta* **1985**, *100*, 41.
(35) Cedeno, D. L; Weitz, E. To be published.